Available online at www.sciencedirect.com

ScienceDirect

Journal of Computational and Applied Mathematics 209 (2007) 109–131

JOURNAL OF COMPUTATIONAL AND APPLIED MATHEMATICS

www.elsevier.com/locate/cam

A finite volume scheme for a model coupling free surface and pressurised flows in pipes☆

C. Bourdarias*, S. Gerbi

Université de Savoie, LAMA, GM^3*, 73376 Le Bourget-du-Lac Cedex, France*

Received 16 May 2005; received in revised form 21 October 2006

Abstract

A model is derived for the coupling of transient free surface and pressurized flows. The resulting system of equations is written under a conservative form with discontinuous gradient of pressure. We treat the transition point between the two types of flows as a free boundary associated to a discontinuity of the gradient of pressure. The numerical simulation is performed by making use of a Roe-like finite volume scheme that we adapted to such discontinuities in the flux. The validation is performed by comparison with experimental results.

MSC: 35L50; 35L65; 35Q35; 65M99; 76M12; 76Q05

Keywords: Water transients in pipes; Free-surface flows; Pressurised flows; Finite volume schemes; Roe scheme

1. Introduction

In this paper we are interested in flows occurring in closed pipes. It may happen that some parts of the flow are free surface (this means that only a part of the section of the pipe is filled) and other parts are pressurised (this means that all the section of the pipe is filled see Fig. 1). The phenomenon of transition from free surface to pressurised flow occurs in many situations as storm sewers, waste or supply pipes in hydroelectric installations. It can be induced by sudden changes in the boundary conditions (failure of a pumping station, rapid change of the discharge, blockage of the line, etc.). During the transition, the excess pressure rise may damage the pipe and cause related problems as ejection of manhole covers, basement flooding. The simulation of such a phenomenon is thus a major challenge and a great amount of works was devoted to it these last years (see [5,17,21,2] for instance).

Let us thus recall the current and previous works in this research field by a partial state of the art review. Cunge and Wegner [4] studied the pressurised flow in a pipe as if it were a free-surface flow by assuming a narrow slot to exist in the upper part of the tunnel, the width of the slot being calculated to provide the correct sonic speed. This approach has been credited to Preissmann. Later, Cunge [3] conducted a study of translation waves in a power canal containing a series of transitions, including a siphon. Pseudoviscosity methods were employed to describe the movement of bores in open-channel reaches. Wiggert [23] studied the transient flow phenomena and his analytical considerations included

☆ This work was fully granted by the Center in Hydraulics Engineering of Electricité De France (CIH-EDF).

* Corresponding author.

E-mail addresses: christian.bourdarias@univ-savoie.fr (C. Bourdarias), stephane.gerbi@univ-savoie.fr (S. Gerbi).

0377-0427/$ - see front matter © 2006 Elsevier B.V. All rights reserved.
doi:10.1016/j.cam.2006.10.086

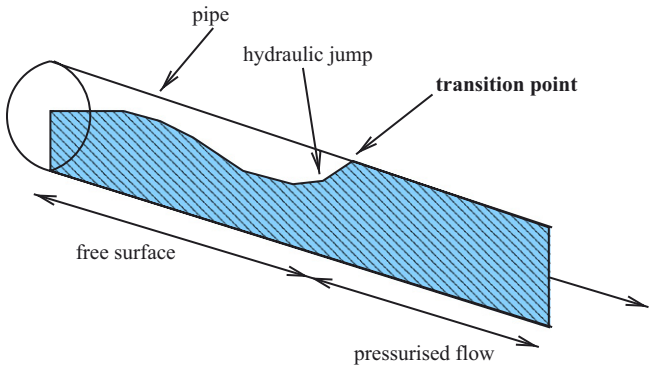

Fig. 1. Mixed flow: free surface and pressurised.

open-channel surge equations that were solved by the method of characteristics. He subjected it to subcritical flow conditions. His solution resulted from applying a similarity between the movement of a hydraulic bore and an interface (that is, a surge front wave). Following Wiggert's model, Song et al. [20] developed two mathematical models of unsteady free-surface/pressurised flows using the method of characteristics (specified time and space) to compute flow conditions in two flow zones. They showed that the pressurised phenomenon is a dynamic shock requiring a full dynamic treatment even if inflows and other boundary conditions change very slowly. However, the Song models do not include the bore presence in the free-surface zone. Hamam and McCorquodale [13] proposed a rigid water column approach to model the mixed flow pressure transients. This model assumes a hypothetical stationary bubble across compression and expansion processes. Li and McCorquodale [15] extended the rigid water column approach to allow for the transport of the trapped air bubble. Recently, Fuamba [8] proposed a model for the transition from a free-surface flow to a pressurised one in a way very close to ours. He wrote the conservation of mass, momentum and energy through the transition point and proposed a laboratory validation of his model. In the last few years, numerical models mainly based on the Preissmann slot technique have been developed to handle the flow transition in sewer systems. Implementing the Preissmann slot technique has the advantage of using only one flow type (free-surface flow) throughout the whole pipe and of being able to easily quantify the pressure head when pipes pressurise. Let us specially mention the work of Garcia-Navarro et al. [11] in which an implicit method based on the characteristics has been proposed and successfully tested on the Wiggert test.

The Saint Venant equations, which are written in a conservative form, are usually used to describe free-surface flows of water in open channels. As said before, they are also used in the context of mixed flows (i.e., either free surface or pressurized) using the artifice of the Preissmann slot [21,2]. On the other hand, the commonly used model to describe pressurized flows in pipes is the system of the Allievi equations [21]. This system of first order partial differential equations cannot be written under a conservative form since this model is derived by neglecting some acceleration terms. This non-conservative formulation is not appropriate for a finite volume discretization and also for a good approximation of the transition between the two types of flows since we are not able to write conservations of appropriate quantities such as momentum and energy. Then, it appears that a "unified" modellisation with a common set of conservative variables (see below) could be of a great interest for the coupling between free-surface and pressurised flows and its numerical simulation could be more effective.

The aim of this paper is: (i) to propose a system of equations written in a conservative form and modelling both types of flows, (ii) describe an explicit finite volume discretisation to solve these equations numerically, (iii) validate the model by comparison with experimental data. Notice that we do not claim that we take into account all the complexity of the physics: we should deal for instance, with entrapment of air bubbles.

In the first part, we derive from the compressible Euler equations an alternative model to the Allievi equations, under a conservative form (following the derivation of the Saint Venant equations). We state some properties of the model such as the conservation of steady states and the existence of an energy for the two types of flows. We show how this model can be connected to the Saint Venant equations through a pressure term with discontinuous gradient via a common set of conservative unknowns. In the second part, the numerical simulation is performed by making use

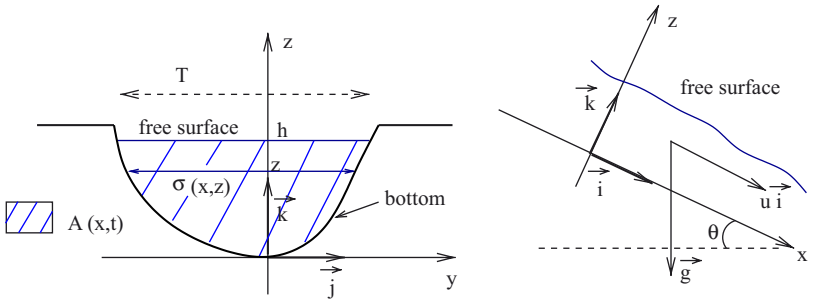

Fig. 2. Free-surface flow in an open channel.

of a Roe-like explicit finite volume scheme adapted to discontinuities of the flux gradient occurring in the treatment of the transitions between free-surface and pressurised flows. Let us notice that with this type of unique conservative formulation for the two types of flows, we are able to deal with flows for which it exists more that one transition point unlike Song et al. [20] with a totally dynamic treatment of these transition points as Fuamba mentions it [8].

2. A conservative model for dual flows

Before we write the dual model, let us briefly recall some features about the Saint Venant equations for the modellisation of free-surface flows in channels.

2.1. Saint Venant equations revisited

The system of Saint Venant for flows in an open channel can be written as

$$\partial_t A + \partial_x Q = 0, \tag{1}$$

$$\partial_t Q + \partial_x \left(\frac{Q^2}{A} + g I_1 \cos\theta(x) \right) = g A(\sin\theta - S_f) + g I_2 \cos\theta(x). \tag{2}$$

The unknowns are the cross-sectional flow area $A = A(x,t)$, and the discharge $Q = Au$ where u is the mean value of the speed over the cross-section in the x-axis direction (see Fig. 2 for the notations).

The other terms are $gI_1\cos\theta(x)$, term of hydrostatic pressure with $I_1 = \int_0^y (h-z)\,\sigma(x,z)\,\mathrm{d}z$ and gI_2, pressure source term induced by the changes of the geometry, with $I_2 = \int_0^h (h-z)\partial_x\sigma(x,z)\,\mathrm{d}z$, where $\sigma(x,z)$ is the width of the cross-section at position x and at height z over the bottom.

Let us remark that $\sigma(x,h) = T$, width of the free surface, and that, from the definition of I_1, we have $I_1(A) = A\overline{y}$ where $\overline{y}$ is the distance between the centre of mass and the free surface of water. In addition we have

$$\frac{\partial I_1}{\partial A} = A\frac{\partial h}{\partial A} = \frac{A}{T}.$$

Notice that since we are not supposing that the slope of the channel $\theta(x)$ is small the usual term of hydrostatic pressure I_1 is replaced by $I_1\cos\theta(x)$.

This system can be derived from the incompressible Euler equations by taking mean values in sections orthogonal to the main flow axis. The free surface is advected by the flow and is assumed to be horizontal in the y direction. The distribution of the pressure is supposed to be hydrostatic: this means that the acceleration of a particle in the plane orthogonal to a streamline is zero. The pressure law writes

$$P(x,y,z) = P_a + \rho g(h(x) - z)\cos\theta(x), \tag{3}$$

where P_a, pressure at the free surface, is usually defined as zero. The terms I_1 and I_2 arise from the computation of the averaged gradient pressure term in a section. In the case of an uniform geometry of the channel (which may be a

pipe, of course) we have $I_2 = 0$ and this is assumed in the sequel. The friction term S_f is assumed to be given by the Manning–Strickler law (see [21]):

$$S_f = K(A)u|u| \quad \text{with } K(A) = \frac{1}{K_s^2 R_h(A)^{4/3}}, \tag{4}$$

where $K_s > 0$ is the Strickler coefficient, depending on the material, and $R_h(A)$ is the so-called hydraulic radius given by $R_h(A) = \frac{A}{P_m}$, P_m being the wet perimeter (length of the part of the channel's section in contact with the water).

A standard computation leads to the following result:

Theorem 1. *System* (1)–(2) *is strictly hyperbolic for* $A(x,t) > 0$. *It admits a mathematical entropy*:

$$E(A, Q, Z) = \frac{Q^2}{2A} + gAZ + gA(h(A) - \overline{y}) = \frac{Au^2}{2} + gAZ + gAh(A) - gI_1(A)$$

which satisfies the entropy inequality:

$$\partial_t E + \partial_x[u(E + gI_1)] \leqslant -gAK(A)u^2|u|.$$

For smooth solutions, the velocity u satisfies:

$$\partial_t u + \partial_x\left(\frac{u^2}{2} + gh(A) + gZ\right) = -gK(A)u|u|. \tag{5}$$

Let Ψ be the quantity $\frac{u^2}{2} + gh(A) + gZ$, called the total head. System (1)–(2) admits a family of smooth steady states characterized by the relations:

$$Q = Au = Q_0,$$

$$u = u(x) \quad \text{and} \quad \frac{\mathrm{d}\Psi}{\mathrm{d}x} = -gK(A)u|u|,$$

where Q_0 is an arbitrary constant.

2.2. A conservative model for unsteady pressurized flows in closed pipes

Using the same mathematical technique as above, we derived the new conservative model for pressurised flows from the 3D system of compressible Euler equations by integration over sections orthogonal to the flow axis. The equation for conservation of mass and the first equation for the conservation of momentum are

$$\partial_t \rho + \mathrm{div}(\rho \vec{U}) = 0, \tag{6}$$

$$\partial_t(\rho u) + \mathrm{div}(\rho u \vec{U}) = F_x - \partial_x P \tag{7}$$

with the speed vector $\vec{U} = u\vec{i} + v\vec{j} + w\vec{k} = u\vec{i} + \vec{V}$, where the unit vector $\vec{i}$ is along the main axis (see Fig. 3). ρ is the density of the water.

We use the Boussinesq pressure law (as in [8] for instance):

$$P = P_a + \frac{1}{\beta}\left(\frac{\rho}{\rho_0} - 1\right), \tag{8}$$

where ρ_0 is the density at the atmospheric pressure P_a and β the coefficient of compressibility of the water. It is easily obtained from the definition of the bulk modulus of elasticity [21]:

$$K = -\frac{\mathrm{d}P}{\mathrm{d}V/V} = \frac{\mathrm{d}P}{\mathrm{d}\rho/\rho} \tag{9}$$

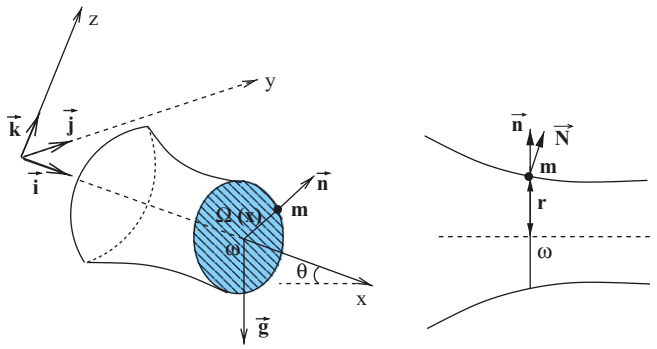

Fig. 3. Pressure flow in a pipe.

for any volume V of liquid, where $K = 1/\beta$. Exterior strengths $\vec{F}$ are the gravity $\vec{g}$ and the friction $-S_f\,\vec{i}$ with S_f still given by (4). We denote $\theta(x)$ the slope of the pipe at position x. Then Eqs. (6)–(7) become

$$\partial_t \rho + \partial_x(\rho u) + \mathrm{div}_{(y,z)}(\rho \vec{V}) = 0, \tag{10}$$

$$\partial_t(\rho u) + \partial_x(\rho u^2) + \mathrm{div}_{(y,z)}(\rho u \vec{V}) = \rho g(\sin\theta - S_f) - \frac{\partial_x \rho}{\beta \rho_0}. \tag{11}$$

Assuming that the pipe is infinitely rigid, Eqs. (10)–(11) are integrated over a cross-section $\Omega(x)$ with area $A(x)$.

Overlined letters represent averaged quantities over $\Omega(x)$. For the first equation we have successively, with the approximation $\overline{\rho u} \simeq \overline{\rho}\,\overline{u}$:

$$\int_{\Omega(x)} \partial_t \rho = \partial_t \int_{\Omega(x)} \rho,$$
$$\int_{\Omega(x)} \partial_x(\rho u) = \partial_x(\overline{\rho}\,\overline{u} A) - \int_{\partial\Omega(x)} \rho u \partial_x \vec{m} \cdot \vec{n},$$
$$\int_{\Omega(x)} \mathrm{div}_{(y,z)}(\rho \vec{V}) = \int_{\partial\Omega(x)} \rho \vec{V} \cdot \vec{n},$$

where $m \in \partial\Omega$, $\vec{m}$ stands for $\overrightarrow{Om}$ and $\vec{n} = \frac{\vec{m}}{|\vec{m}|}$ is the outward unit vector at the point m in the Ω-plane (see Fig. 3). Then, from the waterproof condition $\vec{U} \cdot \vec{N} = 0$ on $\partial\Omega$ we get easily:

$$(u\partial_x \vec{M} - \vec{V}) \cdot \vec{n} = 0 \quad \text{on } \partial\Omega$$

and the following equation for the conservation of mass:

$$\partial_t(\overline{\rho} A) + \partial_x(\overline{\rho}\,\overline{Q}) = 0.$$

$A = A(x)$ is the surface area of a section normal to the pipe axis at position x, $\overline{Q} = A\overline{u}$ is the discharge of the liquid (with the average velocity $\overline{u}$). Next, with the approximations $\overline{\rho u} \simeq \overline{\rho}\,\overline{u}$ and $\overline{\rho u^2} \simeq \overline{\rho}\,\overline{u}^2$, the same procedure applied to (7) gives the conservation law for the momentum:

$$\partial_t(\bar{\rho}\bar{Q}) + \partial_x\left(\bar{\rho}\frac{\bar{Q}^2}{A} + c^2\bar{\rho}A\right) = g\bar{\rho}A(\sin\theta - S_f) + c^2\bar{\rho}\frac{\mathrm{d}A}{\mathrm{d}x},$$

where

$$c^2 = \frac{1}{\beta\rho_0}. \tag{12}$$

Omitting the overlined notations, we get finally the following system written in a conservative form for the unknowns $M = \rho A$, $D = \rho Q$:

$$\partial_t(M) + \partial_x(D) = 0, \tag{13}$$

$$\partial_t(M) + \partial_x\left(\frac{D^2}{M} + c^2\rho M\right) = \rho g M(\sin\theta - S_f) + c^2\frac{M}{A}\frac{\mathrm{d}A}{\mathrm{d}x} \tag{14}$$

with S_f given by the Manning–Strickler law (4). The term $\frac{\mathrm{d}A}{\mathrm{d}x}$ is related to the geometry of the pipe and assumed to be zero in the sequel for the sake of simplicity (uniform section). A complete derivation of this model, taking into account the deformations of the pipe, and a spatial second order finite volume method with Roe's numerical flux in a linearly implicit version is presented in [1]. The preceding system satisfies the following properties:

Theorem 2. *System* (13)–(14) *is strictly hyperbolic. It admits a mathematical entropy*:

$$E(M, D, Z) = \frac{D^2}{2M} + gMZ + c^2 M\ln M$$

which satisfies the entropy inequality:

$$\partial_t E + \partial_x[u(E + c^2\ln M)] \leqslant -gMK(A)u^2|u|.$$

Moreover, for smooth solutions, the velocity u satisfies:

$$\partial_t u + \partial_x\left(\frac{u^2}{2} + gZ + c^2\ln M\right) = 0. \tag{15}$$

Let Ψ be the quantity $\frac{u^2}{2} + c^2\ln M + gZ$, here again called the total head. System (13)–(14) admits a family of smooth steady states characterized by the relations:

$$D = D_0,$$

$$u = u(x) \quad \text{and} \quad \frac{\mathrm{d}\Psi}{\mathrm{d}x} = -gK(A)u|u|, \tag{16}$$

where D_0 is an arbitrary constant.

Remark 3. If we define the water head by $h = \frac{P-P_0}{\rho_0 g}$, the linearised version (8) gives $h = \frac{\rho-\rho_0}{\beta\rho_0^2 g} = c^2\frac{\rho-\rho_0}{\rho_0 g}$. But from (9) we deduce rather $gh = c^2\ln\frac{\rho A}{\rho_0 A} = c^2\ln\frac{\rho}{\rho_0}$, thus (16) is still valid if we define the total head by $\frac{u^2}{2} + g\,h + g\,Z$ in a more classical way.

2.3. Dual model

The two preceding models, for the free-surface flows (1)–(2) and for the pressurised flows (13)–(14), are written under a conservative form and are formally very close to each other. The main difference arises from the pressure laws (3) and (8) and of course, the set of unknowns. This proximity leads us to use a common couple of conservative variables in order to write a single formulation.

Let us consider first a pressurised flow. We define an "FS-equivalent" wet area (FS for Free Surface) A_{eq} through the relation:

$$M = \rho A_{\max} = \rho_0 A_{\mathrm{eq}},$$

where $A_{\max}$ is the cross-sectional area, and a "FS-equivalent discharge" Q_{eq} by

$$D = \rho Q = \rho_0 Q_{\mathrm{eq}} \quad \text{or} \quad Q_{\mathrm{eq}} = A_{\mathrm{eq}}u.$$

Dividing (13)–(14) by ρ_0 we get

$$\partial_t A_{\text{eq}} + \partial_x Q_{\text{eq}} = 0,$$
$$\partial_t Q_{\text{eq}} + \partial_x \left(\frac{Q_{\text{eq}}^2}{A_{\text{eq}}} + c^2 A_{\text{eq}} \right) = g A_{\text{eq}} \sin\theta - g K \frac{Q_{\text{eq}}|Q_{\text{eq}}|}{A_{\text{eq}}}.$$

For a free-surface flow and at a transition point we have obviously $A = A_{\text{eq}}$ and $Q = Q_{\text{eq}}$ with the above definition of A_{eq} and Q_{eq}. Therefore, in the sequel $U = (A, Q)$ denotes the state vector for both flow types.

The dual model thus writes

$$\partial_t A + \partial_x Q = 0, \tag{17}$$

$$\partial_t Q + \partial_x \left(\frac{Q^2}{A} + p(x, A, E) \right) = g A \sin\theta - g K(A, E) \frac{Q|Q|}{A}, \tag{18}$$

where E denotes the "state" of the current point x (free surface: $E = FS$, or pressurised: $E = \text{Press}$) and where the pressure law term writes

$$\begin{cases} p(x, A, E) = g I_1(A) \cos\theta(x) & \text{if } E = FS, \\ p(x, A, E) = g I_1(A_{\max}) \cos\theta(x) + c^2 (A - A_{\max}) & \text{if } E = \text{Press}, \end{cases} \tag{19}$$

and the friction term writes

$$\begin{cases} K(A, E) = \dfrac{1}{K_s^2 R_h(A)^{4/3}} & \text{if } E = FS, \\ K(A, E) = \dfrac{1}{K_s^2 R_h(A_{\max})^{4/3}} & \text{if } E = \text{Press}. \end{cases} \tag{20}$$

The mere value of A is neither sufficient to determine the pressure law nor the coefficient K in the friction term, except in the case $A \geqslant A_{\max}$ (the flow is necessarily pressurised). If $A < A_{\max}$ the flow may be a free-surface flow or a pressurised flow but in depression.

Thus the dual model writes in conservative form

$$\partial_t U + \partial_x F(x, U) = G(x, U),$$

where the unknown state, the flux vector and the source term write respectively:

$$U = \begin{pmatrix} A \\ Q \end{pmatrix}, \quad F(x, U) = \begin{pmatrix} Q \\ \dfrac{Q^2}{A} + p(x, A, E) \end{pmatrix},$$

and

$$G(x, U) = \begin{pmatrix} 0 \\ g A \sin\theta - g K(A, E) \dfrac{Q|Q|}{A} \end{pmatrix}.$$

Let us remark that from the momentum conservation equations (2) and (14) and the friction law (4), the pressure and the friction term are continuous through a transition point.

In each open set in the (x, t) plane, avoiding a transition point, the system is strictly hyperbolic since $DF(x, U) = \begin{pmatrix} 0 & 1 \\ c^2 - u^2 & 2u \end{pmatrix}$ with $u = \frac{Q}{A}$ (average velocity along the flow axis), $c = \sqrt{g \frac{A}{T} \cos(\theta)}$ in case of a free-surface flow and $\sqrt{\frac{1}{\rho_0 \beta}}$ else. The eigenvalues are $\lambda = u \pm c$ and the associated right eigenvectors are $r = \begin{pmatrix} 1 \\ u \pm c \end{pmatrix}$.

The transition points from a type of flow to another are of course, unknowns of the problem. Notice that $p(x, A, E)$ have a discontinuous derivative with respect to x (gradient of pressure) at each transition point. Such a discontinuity is "severe" in the sense that the magnitude of the eigenvalues changes drastically through this point.

Fig. 4 gives, in the case of a rectangular pipe, the behaviour of the pressure and the sound speed with respect to A and the "state variable" E.

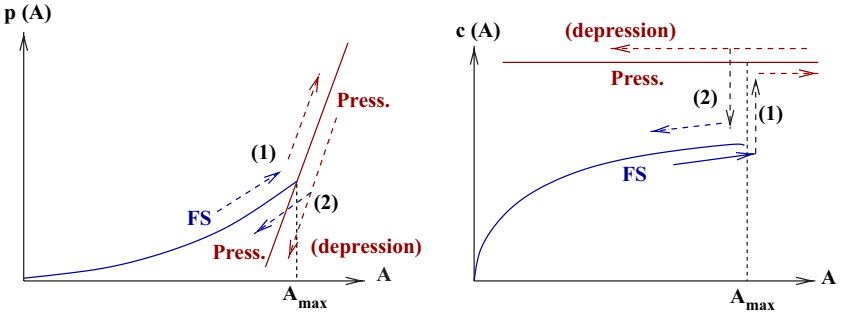

Fig. 4. Pressure law and sound speed in the case of a rectangular pipe. Trajectory (1) corresponds to a pressurization. Trajectory (2) depends on the state of the flow around (see Section 3.5).

3. Finite volume discretisation

3.1. Discretisation of the space domain

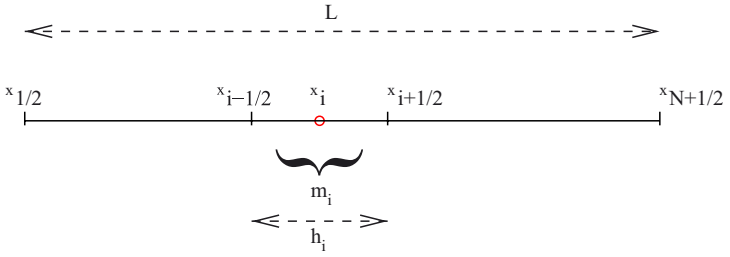

The spatial domain is a pipe of length L. The main axis of the pipe is divided in N meshes $m_i = [x_{i-1/2}, x_{i+1/2}]$, $1 \leqslant i \leqslant N$. Δt denotes the timestep at time t^n and we set $t_{n+1} = t_n + \Delta t$.

The discrete unknowns are $U_i^n = \begin{pmatrix} A_i^n \\ Q_i^n \end{pmatrix}$ $\quad 1 \leqslant i \leqslant N, \quad 0 \leqslant n \leqslant n_{\max}$. The upstream and downstream boundary states U_0^n, U_{N+1}^n are associated to fictive meshes denoted m_0 and m_{N+1}.

3.2. Principle of explicit first order Roe scheme

In this section, we propose a finite volume discretisation of Eqs. (17)–(20) by firstly adapting a well balanced scheme using the upwinding of the source terms due to the slope of the duct as done by LeRoux et al. [12,18] and Gallouet et al. [10,9], secondly by defining a criterion to follow the evolution of the transition points.

Following LeRoux et al. [12,18] we use a piecewise constant function to approximate the bottom of the pipe. Adding the equation $\partial_t Z = 0$ related to the altitude of the bed ($\sin\theta = \partial_x Z$), we note W the conservative variable $(Z, A, Q)^{\mathrm{t}}$ and we get the following system in a non-conservative form:

$$\partial_t W + \partial_x \Phi(x, W) + gA\partial_x Z = TS(W) \tag{21}$$

with

$$\Phi(x, W) = \begin{pmatrix} 0 \\ Q \\ \dfrac{Q^2}{A} + p(x, A) \end{pmatrix}, \quad TS(W) = \begin{pmatrix} 0 \\ 0 \\ -gK(A)\dfrac{Q|Q|}{A} \end{pmatrix}.$$

Such an approximation of the topography introduces a stationary wave for each local Riemann problem at the interfaces $x_{i+1/2}$.

As the possibly discontinuous slope $\theta(x)$ appears in the pressure term $p(x, A)$, we use a piecewise constant function to approximate the slope of the pipe and the same treatment as the bottom topography is performed by using the equation $\partial_t \cos\theta(x) = 0$. A stationary wave for the slope is then added in the following Riemann problem. For the sake of simplicity in the derivation of the following formula, we do not keep track of this point.

Let W_i^n be an approximation of the mean value of W on the mesh m_i at time t_n. Integrating the above equations over $]x_{i-1/2}, x_{i+1/2}[\times[t_n, t_{n+1}[$ we deduce a Finite Volume scheme written as follows:

$$W_i^{n+1} = W_i^n - \frac{\Delta t}{h_i}(\Phi(W^*_{i+1/2}(0^-, W_i^n, W_{i+1}^n)) - \Phi(W^*_{i-1/2}(0^+, W_{i-1}^n, W_i^n))) + TS(W_i^n),$$

where $W^*_{i+1/2}(\xi = x/t, W_i, W_{i+1})$ is the exact or approximate solution to the Riemann problem at interface $x_{i+1/2}$ associated to the left and right states W_i and W_{i+1}. Notice that the topography does not appear explicitly in this formulation ($\partial_x Z = 0$ on $]x_{i-1/2}, x_{i+1/2}[$) but contributes to the computation of the numerical flux. Following Gallouët et al. [9] we compute $W^*_{i+1/2}(0^-, W_i, W_{i+1})$ using an approximate Riemann solver described in the next two subsections.

In order to obtain the numerical scheme to solve Eq. (21), we have to treat two types of interfaces located at the point $x_{i+1/2}$: the first one is a non-transition point, that is, when the flow on the left and on the right sides of the interface is of the same type. The second one is a transition point, that is when the flow changes of type through the interface.

3.3. Case of a non-transition point

Denote

$$B(x, W) = \begin{pmatrix} 0 & 0 & 0 \\ 0 & 0 & 1 \\ gA & c(A)^2 - u^2 & 2u \end{pmatrix}$$

the convection matrix associated to the non-conservative form (21). In this configuration, $W^*_{i+1/2}(\xi = x/t, W_i, W_{i+1})$ is the exact solution to the linear Riemann problem:

$$\begin{cases} \partial_t W + \tilde{J}\partial_x W = 0, \\ W = (Z, A, Q) = \begin{cases} W_l = (Z_l, A_l, Q_l) & \text{if } x < 0, \\ W_r = (Z_r, A_r, Q_r) & \text{if } x > 0 \end{cases} \end{cases} \tag{22}$$

with $(W_l, W_r) = (W_i, W_{i+1})$ and $\tilde{J} = \tilde{J}(W_l, W_r) = B(x_{i+1/2}, \frac{W_l + W_r}{2})$.

$\tilde{J}$ has the eigenvalues $\lambda_1 = 0$, $\lambda_2 = \tilde{u} - \tilde{c}$ and $\lambda_3 = \tilde{u} + \tilde{c}$ with $\tilde{A} = \frac{A_l + A_r}{2}$, $\tilde{u} = \frac{Q_l + Q_r}{A_l + A_r}$ and in the case of a free-surface flow, $\tilde{c} = \sqrt{g\frac{\tilde{A}}{T(\tilde{A})}\cos\theta}$ and in the case of a pressurised flow $\tilde{c} = c = \sqrt{\frac{1}{\beta\rho_0}}$. The eigenvectors are:

$$\tilde{r}_1 = \begin{pmatrix} \tilde{c}^2 - \tilde{u}^2 \\ -g\,\tilde{A} \\ 0 \end{pmatrix}, \quad \tilde{r}_2 = \begin{pmatrix} 0 \\ 1 \\ \tilde{u} - \tilde{c} \end{pmatrix} \quad \text{and} \quad \tilde{r}_3 = \begin{pmatrix} 0 \\ 1 \\ \tilde{u} + \tilde{c} \end{pmatrix}.$$

The solution of the Riemann problem (22) consists in four constant states connected by shocks propagating along the lines $\xi = x/t = \lambda_i$. Since the values of the altitude Z are known, we are looking for the states on each sides of the line $\xi = 0$ denoted by (AM, QM) for the left side and (AP, QP) for the right side (see Fig. 5). Moreover, as the third component of $\tilde{r}_1$ is null, the discharge Q is continuous through the line $\xi = 0$. Thus $QM = QP$. In the sequel, we denote QMP this value. By a straightforward computation, we have the three cases:

Case 1: if $\tilde{u} > \tilde{c}$

$$\begin{aligned} &AM = A_l, \\ &QMP = Q_l, \\ &AP = AM + \frac{g\tilde{A}}{\tilde{u}^2 - \tilde{c}^2}(Z_r - Z_l). \end{aligned}$$

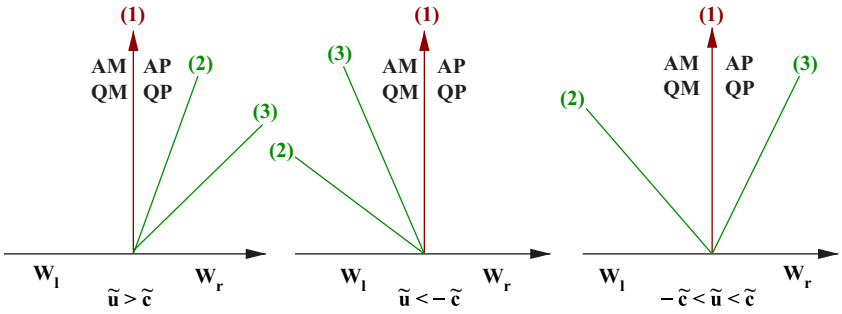

Fig. 5. Solution of the Riemann problem (22). The number of the lines corresponds to the eigenvalues.

Case 2: if $\tilde{u} < -\tilde{c}$

$$AM = A_r,$$
$$QMP = Q_r,$$
$$AM = AP - \frac{g\tilde{A}}{\tilde{u}^2 - \tilde{c}^2}(Z_r - Z_l).$$

Case 3: if $-\tilde{c} < \tilde{u} < \tilde{c}$

$$AM = A_l + \frac{g\tilde{A}}{2\tilde{c}(\tilde{c} - \tilde{u})}(Z_r - Z_l) + \frac{\tilde{u} + \tilde{c}}{2\tilde{c}}(A_r - A_l) - \frac{1}{2\tilde{c}}(Q_r - Q_l),$$
$$QMP = Q_l - \frac{g\tilde{A}}{2\tilde{c}}(Z_r - Z_l) + \frac{\tilde{u}^2 - \tilde{c}^2}{2\tilde{c}}(A_r - A_l) - \frac{\tilde{u} - \tilde{c}}{2\tilde{c}}(Q_r - Q_l),$$
$$AP = AM + \frac{g\tilde{A}}{\tilde{u}^2 - \tilde{c}^2}(Z_r - Z_l).$$

Let us mention that in the case of a pressurised flow, since the velocity is always less (in magnitude) that the sound velocity, we are always in the case 3. Adding the altitude in system (21) produced an upwinding term $g\tilde{A}(Z_r - Z_l)$.

The equivalent area A_i^n in the mesh i at the time t_n can thus be updated by the formula:

$$A_i^{n+1} = A_i^n - \frac{\Delta t}{h_i}(QMP_{i+1/2} - QMP_{i-1/2}). \tag{23}$$

Finally, by using the updated value of the equivalent area at time t_{n+1}, A_i^{n+1}, in the cell i and by performing a linearisation around A_i^{n+1} for the friction term we get

$$Q_i^{n+1} = Q_i^n + \frac{\Delta t}{1 + \dfrac{2gK(A_i^{n+1}, E_i^{n+1})|Q_i^n|\Delta t}{A_i^{n+1}}} \times \left\{ \begin{array}{l} -\dfrac{1}{h_i}[F_2(AM_{i+1/2}, QMP_{i+1/2}) - F_2(AP_{i-1/2}, QMP_{i-1/2})] \\ -g\dfrac{|Q_i^n|Q_i^n K(A_i^{n+1}, E_i^{n+1})}{A_i^{n+1}} \end{array} \right\}, \tag{24}$$

where the index 2 indicates the second component of the flux vector F.

3.4. Case of a transition point

We treat this transition point as a free boundary associated to a discontinuity of the gradient of the pressure. The numerical treatment must be coherent with the general case: the constant states on the left and right side of the line

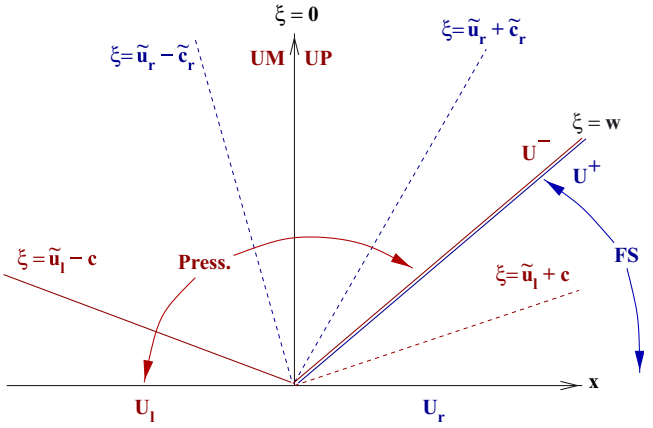

Fig. 6. Pressure state propagating downstream.

$\xi = 0$, respectively, noted $UM = (AM, QM)$ and $UP = (AP, QP)$ are obtained through the resolution of the above linear Riemann problem, but the matrix $\tilde{J}(U_l, U_r)$ is discontinuous (actually piecewise constant).

Assuming that the transition point propagates with a constant speed w during a time step, the half line $x = w\,t$, is the discontinuity line of $\tilde{J}(U_l, U_r)$.

Let us now consider $U^- = (A^-, Q^-)$ and $U^+ = (A^+, Q^+)$ the (unknown) states, respectively, on the left and on the right side of the line $x = w\,t$. Both states U_l and U^- (resp. U_r and U^+) corresponds to the same type of flow. Thus, it makes sense to define averaged matrices in each zone as follows:

- for $x < wt$, we set $\tilde{J}_l = \tilde{J}(U_l, U_r) = DF(\tilde{U}_l)$ with $\tilde{U}_l = \frac{U_l + U^-}{2}$,
- for $x > w\,t$, we set $\tilde{J}_r = \tilde{J}(U_l, U_r) = DF(\tilde{U}_r)$ with $\tilde{U}_r = \frac{U_r + U^+}{2}$.

Then we formally solve two Riemann problems and uses the Rankine–Hugoniot jump condition through the line $x = wt$ which writes

$$Q^+ - Q^- = w(A^+ - A^-), \tag{25}$$

$$F_2(A^+, Q^+) - F_2(A^-, Q^-) = w(Q^+ - Q^-) \tag{26}$$

with $F_2(A, Q) = \frac{Q^2}{A} + p(A)$ (we omit the E-dependency). The unknown states are U^-, U^+, UM, UP and w.

We can consider two couples of "twin cases": pressure state propagating downstream (or upstream) as shown in Fig. 6 and free-surface state propagating downstream (or upstream) as shown in Fig. 7. The direction of the transition point is predicted thanks to the sign of $w_{\text{pred}} = \frac{Q_r - Q_l}{A_r - A_l}$.

The case of a propagating free-surface state appears to be the more complex.

3.4.1. Pressure state propagating downstream (Fig. 6)

On the left side of the line $\xi = wt$ we have a pressurised flow and on the right side we have a free-surface flow, (the speed w of the transition point being positive). Following Song [20] (see also [8]), an equivalent stationary hydraulic jump must occur from a supercritical to a subcritical condition and thus, the characteristics speed satisfies the inequalities:

$$\tilde{u}_r + \tilde{c}_r < w < \tilde{u}_l + c,$$

where c is the sound speed for the pressure flow, $\tilde{u}_l$, $\tilde{u}_r$, and $\tilde{c}_r$ are defined by the same formula obtained in the case of a non-transition point but according to $\tilde{J}_l$ and $\tilde{J}_r$.

Therefore, only the characteristic lines drawn with solid lines are taken into account, indeed they are related to incoming waves with respect to the corresponding space–time area $-\infty < \xi < w$. Conversely, the dotted line $\xi = \tilde{u}_r - \tilde{c}_r$,

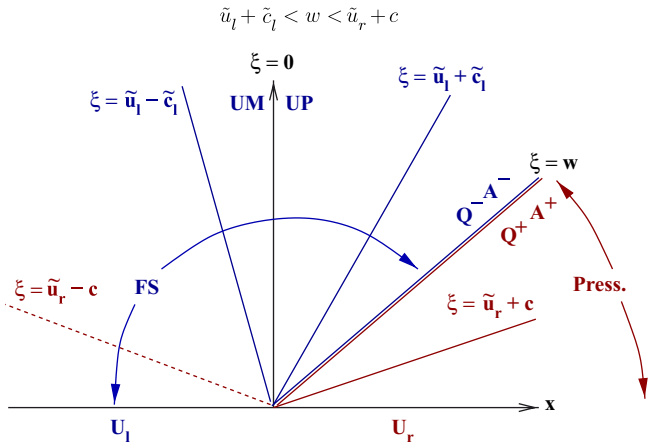

Fig. 7. Free-surface state propagating downstream.

for instance, related to the free-surface zone but drawn in the area of pressurised flow is a "ghost wave" and is not considered. Thus, $U^+ = U_r$ and U_l, U^- are connected through the jumps across the characteristics $\xi = 0$ and $\xi = \tilde{u}_g - c$. Eliminating w in the Rankine–Hugoniot jump relations (25)–(26), we get U^- as the solution to the non-linear system:

$$(Q_r - Q^-)^2 = (A_r - A^-)\,(F_2(A_r, Q_r) - F_2(A^-, Q^-)), \tag{27}$$

$$Q^- - A^-(\tilde{u}_r - c) + \frac{g Z_r \tilde{A}_l}{c + \tilde{u}_l} = Q_l - A_l\,(\tilde{u}_l - c) + \frac{g Z_l \tilde{A}_l}{c + \tilde{u}_l}. \tag{28}$$

This system is solved numerical by a quasi-Newton method implemented in the `minpack` package (see [16]). Finally, we obtain $UP = U^-$, i.e., $AP = A^-$, $QM = QP = QMP = Q^-$, and the jump relation through the stationary wave $\xi = 0$ gives

$$AM = AP - \frac{g \tilde{A}_l (Z_r - Z_l)}{\tilde{u}_l^2 - c^2}.$$

3.4.2. Free-surface state propagating downstream (Fig. 7)

On the left side of the line $\xi = wt$ we have a free-surface flow and on the right side we have a pressurised flow (the speed w of the transition point being positive). Following Song [20] again, the characteristic speed satisfies the inequalities:

$$\tilde{u}_l + \tilde{c}_l < w < \tilde{u}_r + c.$$

There are two incoming characteristic lines with respect to the free-surface area $-\infty < \xi < w$ (actually three with $\xi = 0$) and they can connect the given left state U_l with any arbitrary free-surface state UM. Thus, only one characteristic line ($\xi = \tilde{u}_r + c$) gives any information (it is Eq. (29)) as an incoming characteristic line with respect to the pressurised zone $w < \xi < +\infty$. From the jump relations through the characteristic $\xi = 0$, and after the elimination of w in the Rankine–Hugoniot jump relations (25), (26) we get another equation, namely Eq. (30). It remains to close the system of four unknowns (A^-, Q^-, A^+, Q^+).

Firstly, we use a jump relation across the transition point (with speed w) for the total head $\Psi = \frac{u^2}{2} + g\,h(A) + g\,Z$ arising from Eqs. (5) and (15). Recall that $h(A)$ is the water head (the water height in the case of a free-surface flow and the piezometric level above the bottom of the pipe for the pressurised flow). This relation writes

$$\Psi^+ - \Psi^- = w\,(u^+ - u^-).$$

This relation is equivalent to the one proposed by Whitham [22]:

$$\frac{(u^+ - w)^2}{2g} + h(A^+) = \frac{(u^- - w)^2}{2g} + h(A^-) + \delta h,$$

where the dissipation term δh has to be experimentally determined. In this first approach we neglect it.

Lastly we use the relation:

$$w = w_{\text{pred}}.$$

We have then to solve the non-linear system:

$$(Q_r - Q^+) = (A_r - A^+)\,(\tilde{u}_r + c), \tag{29}$$

$$(Q^+ - Q^-)(Q_r - Q_l) = (A_r - A_l)(F_2(A^+, Q^+) - F_2(A^-, Q^-)), \tag{30}$$

$$\frac{(Q^+)^2}{2(A^+)^2} + gh(A^+) - \frac{(Q^-)^2}{2(A^-)^2} - gh(A^-) = \frac{Q_r - Q_l}{A_r - A_l}\left(\frac{Q^+}{A^+} - \frac{Q^-}{A^-}\right), \tag{31}$$

$$(Q_r - Q_l)(A^+ - A^-) = (Q^+ - Q^-)(A_r - A_l). \tag{32}$$

This system is solved numerically by a quasi-Newton method implemented in the `minpack` package (see [16]).

The states *UM* and *UP* are then obtained by the following identities:

$$AM = A_l + \frac{g\tilde{A}_l(Z_r - Z_l)}{2\tilde{c}_l(\tilde{c}_l - \tilde{u}_l)} + \frac{\tilde{u}_l + \tilde{c}_l}{2\tilde{c}_l}(A^- - A_l) - \frac{1}{2\,\tilde{c}_l}(Q^- - Q_l),$$

$$AP = AM + \frac{g\tilde{A}_l(Z_r - Z_l)}{\tilde{u}_l^2 - \tilde{c}_l^2},$$

$$\begin{aligned} QM = QP = QMP \\ = Q_l + \frac{g\tilde{A}_l(Z_r - Z_l)}{2\tilde{c}_l} + \frac{\tilde{u}_l^2 - \tilde{c}_l^2}{2\tilde{c}_l}(A^- - A_l) - \frac{\tilde{u}_l - \tilde{c}_l}{2\tilde{c}_l}(Q^- - Q_l). \end{aligned}$$

Finally, the updated state A_i^{n+1}, Q_i^{n+1} are obtained by the same relation as in the case of a non-transition point, namely by Eqs. (23), (24).

Let us mention that since the numerical scheme is an explicit one, the time step size at time t_n, namely Δt must be controlled by the mesh size by the usual stability condition of Courant–Friedich–Levy:

$$\Delta t = C\frac{\inf_{i\in\mathbb{Z}} h_i}{\max\{|\tilde{\lambda}^n_{k,i+1/2}|;\ 2\leqslant k\leqslant 3,\ i\in\mathbb{Z}\}}, \quad C\in]0,1[, \tag{33}$$

where $\tilde{\lambda}^n_{k,i+1/2}$ is the kth eigenvalue of $\tilde{J}(U_i^n, U_{i+1}^n)$.

3.5. Updating the state E in a mesh

After the computation of the "pseudo wet area" A_i^{n+1} we need to have a criterion to determine the state of each mesh at time t_{n+1}, and thus, to find the new position of the transition points. Notice that the value of A_i^{n+1} is not always sufficient to conclude: if $A_i^{n+1} \geqslant A_{\max}$ it is clear that the mesh m_i becomes pressurised, on the other hand, if $A_i^{n+1} < A_{\max}$ in a mesh previously pressurised, we do not know a priori if the new state is free surface ($\rho = \rho_0$ and the value of the wetted area is less than $A_{\max}$) or pressurised (in depression, with $\rho < \rho_0$ and the value of the wetted area is equal to $A_{\max}$).

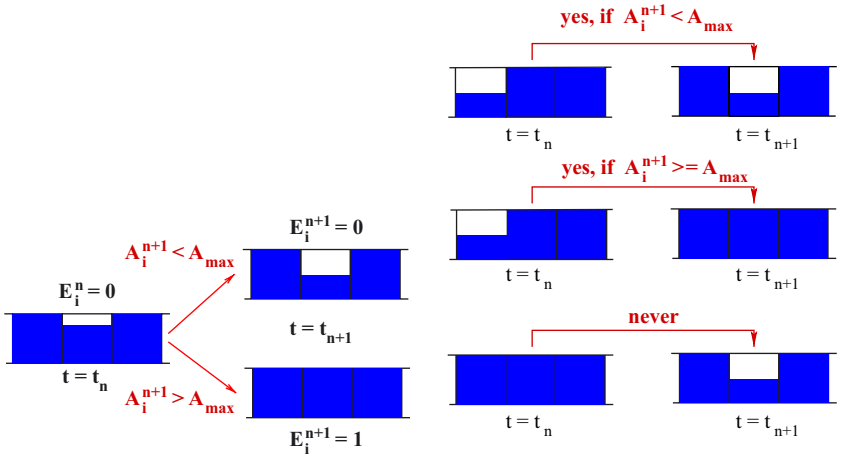

Fig. 8. Updating E.

So far as we do not take into account complex phenomena such that entrapment of air pockets or cavitation and keeping in mind that the CFL condition (33) ensures that a transition point crosses at most one mesh at each time step, we postulate that:

(1) if the mesh m_i is free surface at time t_n, its state at time t_{n+1} is only determined by the value of A_i^{n+1} and it cannot become in depression,
(2) if the mesh m_i is pressurised at time t_n and if $A_i^{n+1} < A_{\max}$, it becomes free surface if and only if at least one adjacent mesh was free surface at time t_n.

We set $E = 1$ for a pressurised flow and $E = 0$ else. Let E_i^n be the known state of the flow in the mesh i at time t_n: we have to find E_i^{n+1}, $1 = 1, \ldots, N$. Thus, our criterion is the following (see Fig. 8):

- if $E_i^n = 0$ then:
  if $A_i^{n+1} < A_{\max}$ then $E_i^{n+1} = 0$, else $E_i^{n+1} = 1$,
- if $E_i^n = 1$:
  if $A_i^{n+1} \geqslant A_{\max}$ then $E_i^{n+1} = 1$, else $E_i^n = E_{i-1}^n \cdot E_{i+1}^n$.

Notice that this procedure allows to distinguish between free-surface flow and pressurised flow in depression when $A_i^{n+1} < A_{\max}$ unlike the Preissmann slot techniques which can treat only pressurised flow with positive pressure of the water.

3.6. Boundary conditions

We recall that the upstream and downstream state vectors (corresponding to $x_{1/2}$ and $x_{N+1/2}$) at time t_n are, respectively, denoted $U_0^n = \begin{pmatrix} A_0^n \\ Q_0^n \end{pmatrix}$ and $U_{N+1}^n = \begin{pmatrix} A_{N+1}^n \\ Q_{N+1}^n \end{pmatrix}$. From a mathematical point of view, we must give as many scalar boundary conditions as incoming characteristic curves. In the case of a subcritical flow, say at the upstream end, $A_0^n = A(0, t_n)$ and $Q_{N+1}^n = Q(L, t_n)$ are given quantities or, more generally, we impose some condition $f_{\text{up}}(A, Q, t) = 0$.

Numerically, the computation of the boundary fluxes (via the resolution of the Riemann problem (22)) requires complete state vectors that one can consider as "exterior" values on fictive meshes. U_0^n and U_{N+1}^n play this role and are supposed to be known at time t_n. Thus, the problem is to determine or estimate the boundary states U_0^{n+1} and U_{N+1}^{n+1}.

The method described below is closely related to those studied by Dubois [6] and Kumbaro [14] (see also [7]). It allows to update the boundary states using known values at the same level time, so it is naturally implicit. Let us recall the original procedure in the case of a subcritical flow at the upstream end, for instance.

We start with given interior vector states U_i^{n+1} $(1 \leqslant i \leqslant N)$ and any given relationship

$$f_{\mathrm{up}}(A_0^{n+1}, Q_0^{n+1}, t_{n+1}) = 0.$$

We have to build a complete boundary state using these data at the same level time and not at the previous one as in the characteristic method. The vector states W_0^{n+1} and W_1^{n+1} are expressed in the basis of eigenvectors of the matrix $\tilde{J}$ in (22) where we assume that $Z_0 = Z_1$ (notice that these eigenvectors depend on the unknown U_0^{n+1}):

$$W_0^{n+1} = \alpha_0^{n+1}\tilde{r}_1 + \beta_0^{n+1}\tilde{r}_2 + \gamma_0^{n+1}\tilde{r}_3 \quad \text{and} \quad W_1^{n+1} = \alpha_1^{n+1}\tilde{r}_1 + \beta_1^{n+1}\tilde{r}_2 + \gamma_1^{n+1}\tilde{r}_3.$$

The method consists of connecting W_0^{n+1} to W_1^{n+1} by an unique jump through the incoming characteristic $x = \tilde{\lambda}_3 t$, thus setting $\alpha_0^{n+1} = \alpha_1^{n+1}$ and $\beta_0^{n+1} = \beta_1^{n+1}$ or equivalently $Q_1^{n+1} - Q_0^{n+1} = (\tilde{u}_{1/2}^{n+1} + \tilde{c}_{1/2})(A_1^{n+1} - A_0^{n+1})$. Then we get U_0^{n+1} as the solution of the non-linear system.

Notice that we do not know a priori if the flow is subcritical at time t_{n+1}, so we have to test this property a posteriori. In case of a negative result, we choose to impose a critical flow. Another difficulty may arises from the occurrence of a transition point: the treatment is similar to the interior case.

4. Numerical validation

In this section, we present our numerical results for the case of a single point pressurised flow, namely the test proposed by Wiggert [23]. The numerical results are then compared with the experimental ones: a very good agreement between them is shown. Another single point pressurised flow is presented: it is the test proposed by Zech et al. [2]. We do not dispose of clear experimental results in Zech's article. Nevertheless the shape of the piezometric line seems to be in agreement by the one obtained by Zech et al.

The case of multiple points pressurised flow is numerically performed for a circular pipe where the upstream prescribed hydrograph produces a wave in the free-surface flow, whereas the downstream discharge is suddenly cut at the time $t = 50$ s, producing a waterhammer. This test was constructed to see if the method could treat such flows and was not performed in a laboratory.

Notice that in the following numerical experiments, the sound speed c for the pressurised part of the flow is a tunable parameter. This is, of course, in contradiction with the theoretical value (12) which corresponds to $c \simeq 1.4 \times 10^3$ m/s. Actually, in a model taking in account the characteristics of the material of a circular pipe, we should rather have (see [21] for instance):

$$c \simeq \frac{c}{\sqrt{1 + \dfrac{\delta}{\beta e E}}},$$

where δ is the diameter of the pipe, e is the wall thickness (assumed here to be constant) and E is the Young's modulus of elasticity for the wall material (in the rigid case $E = +\infty$ gives (12)). Moreover, we should have to deal with the entrapment of air bubbles which have a non-negligible effect (see [13,19] for instance). In the case of the Wiggert's test described in the next subsection, the pipe is a complex structure and the value of c is not really known. According to the experimental data, we were able to propose a value (or a range of values) for c which seems physically relevant. On the contrary, in the Preissmann slot technique [23,11] the value of c is related to an arbitrary value (the width of the slot) and cannot exceed practically 10 m/s, otherwise the method becomes unstable.

4.1. Single point pressurised flow

The following test case, is due to Wiggert [23]. The experimental device (see Fig. 9) is an horizontal 10 m long closed pipe with width 0.51 m and height $H = 0.148$ m. The Manning number is $1/K_s^2 = 0.012\ \mathrm{s/m^{1/3}}$. The initial conditions are a stationary state with the discharge $Q_0 = 0$ and the water level $h_0 = 0.128$ m.

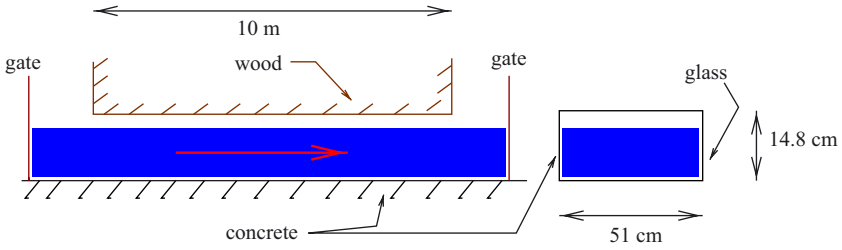

Fig. 9. Experimental device (adapted from Wiggert [23]).

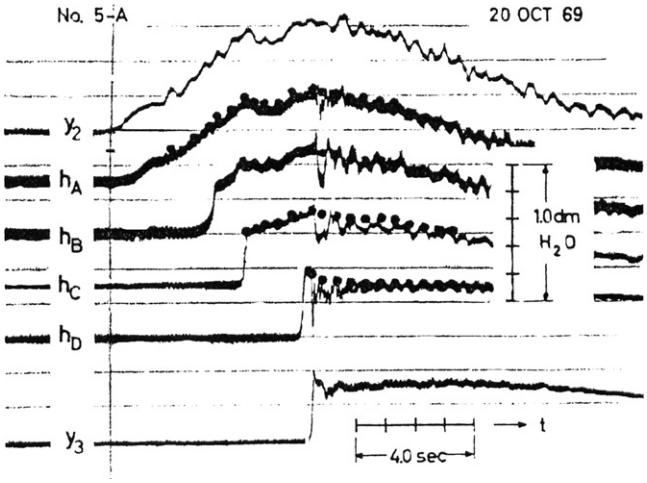

Fig. 10. Wiggert: experimental data. y_2: upstream hydrograph, y_3: downstream hydrograph. h_A, h_B, h_C, h_D: pressure head at 0.5, 3.5, 5.5 and 9.5 m from the tunnel entrance (location of recording instruments) [23].

Then a wave coming from the left side causes the closed channel to pressurise. The upstream condition is a given hydrograph (y_2 in Fig. 10), at the downstream end, a step function is imposed: the water level is kept constant to $h_0 = 0.128$ m until the wave reaches the exit. At this time, the level is suddenly increased (see y_3 in Fig. 10). For the computations, these boundary conditions have been read on Wiggert's article and rebuilt using piecewise polynomial interpolations (Fig. 11).

Let us define the piezometric head by

$$\text{piezo} = z + H + p \quad \text{with} \quad \begin{cases} p = \dfrac{c^2(\rho - \rho_0)}{\rho_0 g} & \text{if the flow is pressurised,} \\ p = h \text{ the water height} & \text{if the flow is free surface.} \end{cases}$$

In Fig. 12, we present the piezometric line computed at 3.5 m from the tunnel entrance (solid curve). Circles represent experimental data read on curve h_B, including maxima and minima points of the oscillating parts. We can observe a very good agreement with the experimental data even for the oscillations. We point out that we did not find in other papers, by authors carrying out the same simulation, a convenient numerical reproduction of these oscillations: they do not treat the dynamical aspect of the pressure flow, in particular when using the Preissmann slot technique [23,11]. On the other hand, we found in Fuamba [8] a similar and interesting approach with a non-conservative formulation and another numerical method (characteristics).

The value of the sound speed c was taken equal to 40 m/s, roughly according to the frequency of the oscillations observed during the phase of total submersion of the tunnel. This low value can be explained by the structure of the tunnel and by bubble flow (see [13] for instance).

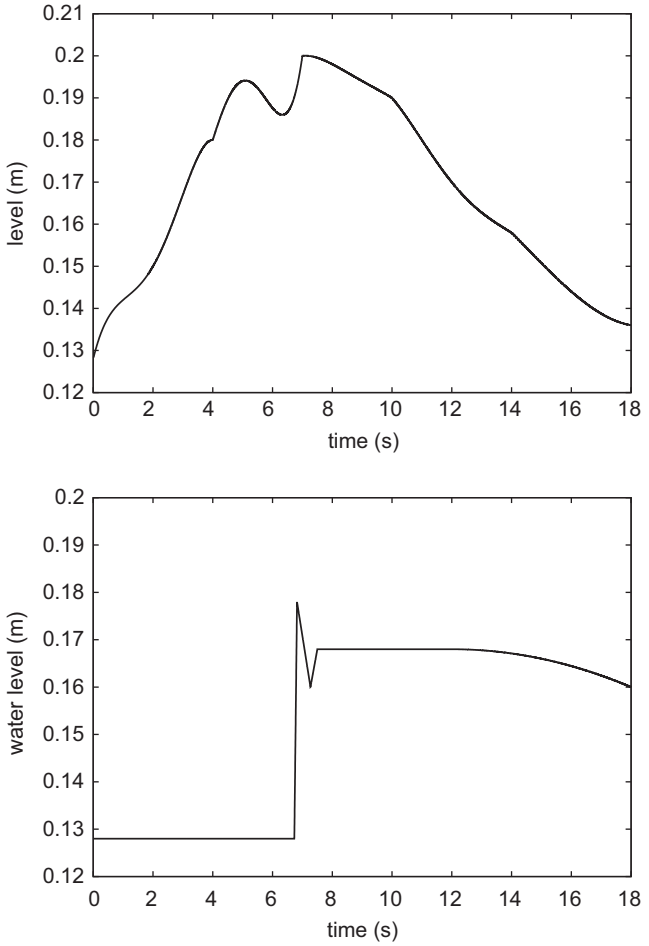

Fig. 11. Wiggert's test: upstream hydrograph (up) and downstream water level (down).

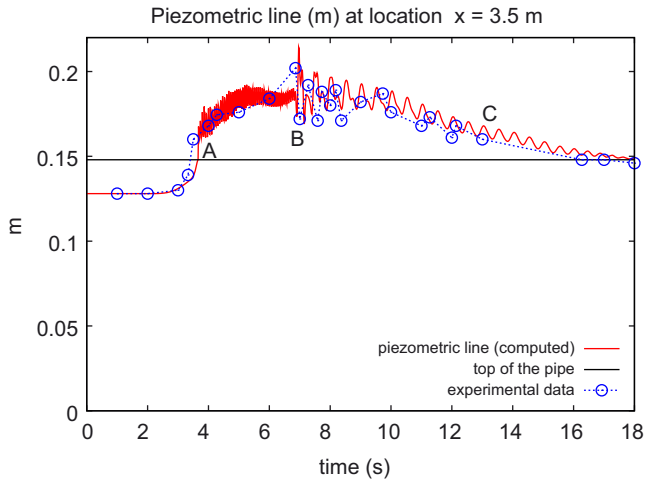

Fig. 12. Piezometric line at location $x = 3.5\,\mathrm{m}$ (corresponding to h_B) with $c = 40\,\mathrm{m/s}$.

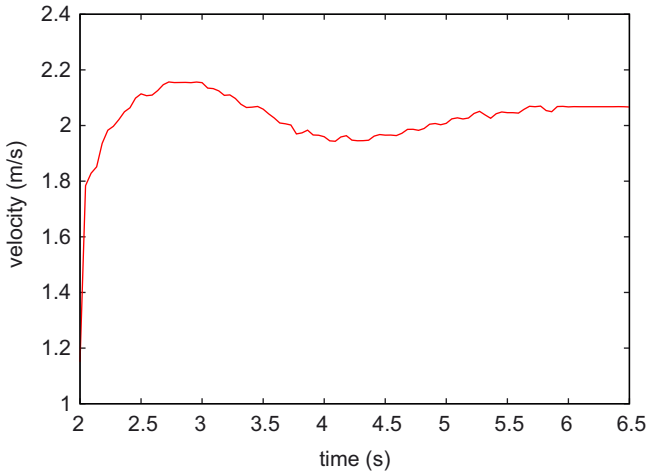

Fig. 13. Velocity of the transition point.

We observe that the front reaches the control point at 3.6 s, in a good agreement with the experimental data (less than 0.15 s late). Let us mention that before it reaches the exit (part AB in Fig. 12) the oscillations of the pressure associated with the moving front reflect between upstream and the front itself (since the free surface is at constant pressure) where the channel is flooded. Beyond point B the oscillations result from the step in the downstream water level and they propagate in the fully pressurized flow (their frequency was estimated using the BC part of the experimental curve).

Fig. 13 gives the evolution of the front's speed. We observe the same behaviour as in [23]: the front quickly attains a maximum speed, decelerates and then slowly accelerate as it approaches the tunnel exit. Moreover, the values are consistent with those of Wiggert. Notice that the speed of the front is not very dependent on the value of c.

Another test case is described by Zech et al. in [2]. It consists in the pressurisation of steep slope circular pipe. Unfortunately, we do not dispose of the exact measures and we do not present this test as a validation of our method but as a representative test of a severe pressurisation.

The experimental set-up features a 12.74 m long perspex pipe with a 145 mm inner diameter. The pipe consists of three parts with bottom slopes 0.01954 m/m (0–3.48 m), 0.01704 m/m (3.48–9.23 m) and 0.01255 m/m (9.23–12.74 m), respectively. The Manning roughness coefficient is $1/K_s^2 = 0.009\,\mathrm{s/m^{1/3}}$. Due to the relatively steep slope of the pipe, free-surface flows at the upstream extremity are almost supercritical while the flow regime at the downstream end depends on the water level. Fast variations of this water level can be obtained by operating an adjustable weir in a downstream tank.

The boundary conditions are the following. At the upstream, a constant discharge of 4.2 l/s is kept. The experiment starts from a steady supercritical flow. The adjustable downstream weir is rapidly raised, supressing the outflow from the downstream tank. As the downstream water level rises, a hydraulic jump is forced into the pipe and migrates upstream. When the jump comes near the upstream end, the downstream weir is abruptly lowered back. This leads to a sudden decrease of the downstream level. A fast transient, in the form of a negative wave returns the flow to its initial conditions.

The hydrograph of the downstream end is presented in Fig. 14. Fig. 15 presents the steady supercritical flow at time $t = 0$ s. Fig. 16 is reproduced from [2]. Fig. 17 presents the piezometric line at the same times as in Fig. 16. We can firstly observe that the conservation of steady states with constant discharge is obtained and secondly that the piezometric lines and the speed of the wave front seem to be in a good agreement with the ones obtained by Zech et al., at least at the qualitative level.

4.2. Multiple points pressurised flow

For this test, we consider a 150 m long circular pipe of diameter 1 m with slope 0.003 m/m. The Manning roughness coefficient is $1/K_s^2 = 0.012\,\mathrm{s/m^{1/3}}$. The simulation starts from a steady state as a free-surface flow with a discharge

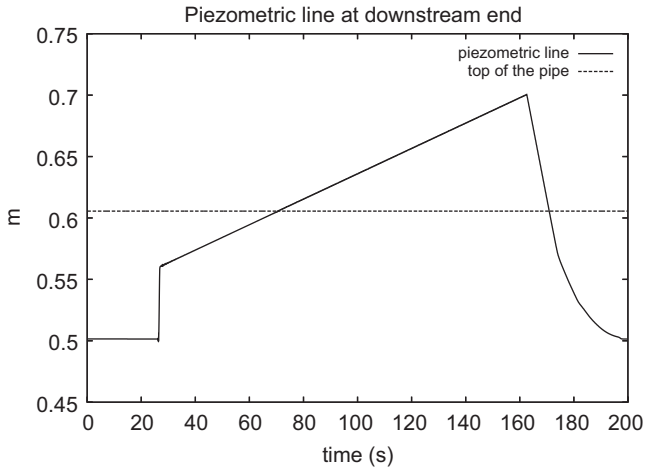

Fig. 14. Prescribed hydrograph at the downstream end of the pipe.

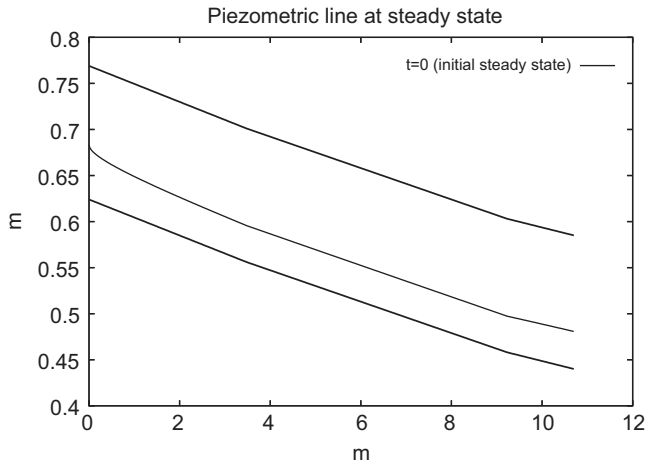

Fig. 15. Supercritical steady state taken as initial condition.

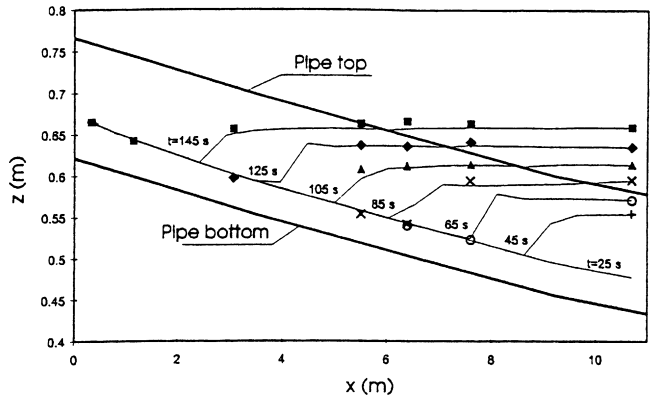

Fig. 16. Results from Capart et al. [2, p. 667].

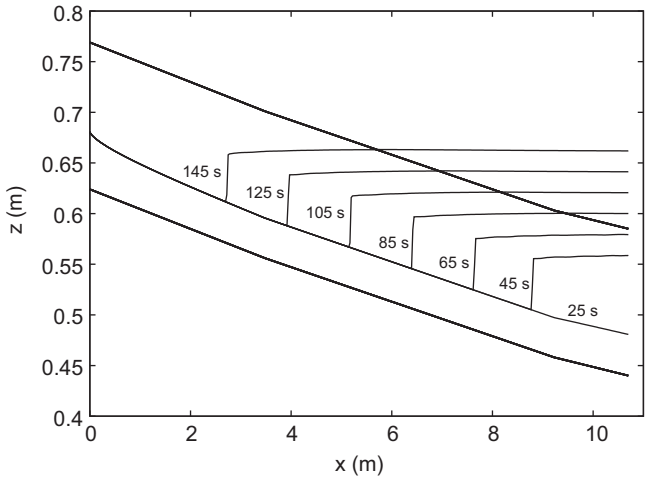

Fig. 17. Results from the code ROEMIX.

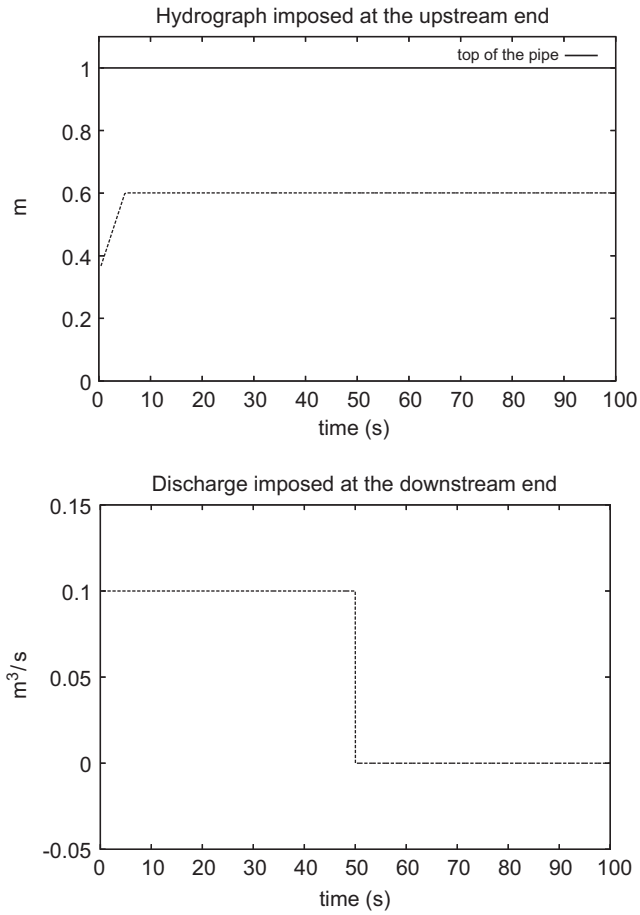

Fig. 18. Multiple transition point test: upstream hydrograph (up) and downstream discharge (down).

$Q = 0.1\,\mathrm{m}^3/\mathrm{s}$ and the water level is chosen as $y = 0.35\,\mathrm{m}$. The boundary condition at the upstream end is a prescribed hydrograph and at the downstream end is a prescribed discharge. Between the time $0 \leqslant t \leqslant 5$ the upstream water level increases linearly between $y = 0.35\,\mathrm{m}$ and $y = 0.6\,\mathrm{m}$. After the time $t = 5\,\mathrm{s}$, the upstream water level is kept constant

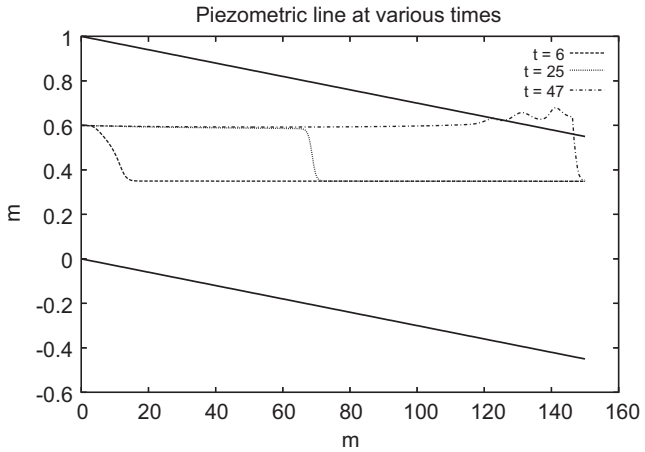

Fig. 19. The free-surface travelling wave from upstream and reaching the top of the pipe.

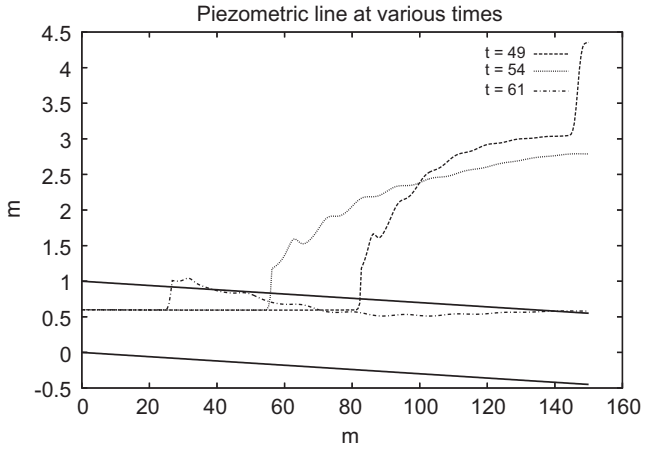

Fig. 20. The waterhammer coming from downstream.

to the value $y = 0.6$ m. Between the time $0 \leqslant t \leqslant 50$, the downstream discharge is kept constant to the initial value $Q = 0.1\ \mathrm{m}^3/\mathrm{s}$ and at the time $t = 50$ s, the discharge is cut in 0.01 s (see Fig. 18).

This type of boundary upstream condition produces a free-surface flow with a wave travelling from the upstream to the downstream. And due to the slope of the pipe, this wave reaches the top of the pipe and produces a two-point pressurised flow (see Fig. 19 to see the profiles of the wave coming from downstream). Let us remark that since from the times $t = 0$ s to $t = 47$ s, the downstream discharge is constant, the pressurised flow is only produced by the downstream boundary condition. This fast speed pressurised flow will reach the downstream end and since the discharge is constant it will produce a first waterhammer.

The profile at the time $t = 47.5$ s shows this waterhammer. Another waterhammer is produced by the sudden cut of the discharge and the profile at the time $t = 50.01$ s shows this second waterhammer. The profile at the time $t = 61$ s shows in fact only a single transition point. A careful analysis of the flow (which is performed by the variable E in the numerical code) shows that after this transition point, the flow is pressurised but in depression. This is the reason why the piezometric line is under the top of the pipe (see Fig. 20 to see these three profiles).

In Fig. 21, we present the mixed final stationary flow.

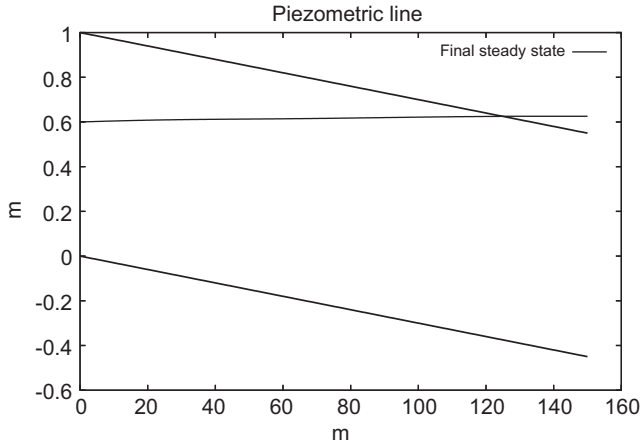

Fig. 21. The final mixed steady-state flow.

One can see (with this test), that the modellisation of mixed flows by the dual model and the proposed numerical resolution method can handle more that only one transition point and also mixed flows with a pressurised flow in depression. The treatment of the transition is fully dynamic.

The numerical method was implemented in Fortran 90 in the code `roemix` which is able to deal also with only free surface or only pressure flows (as well as mixed flows). It was completely validated in these particular cases situations using test cases supplied by the Center in Hydraulics Engineering of Electricité De France (CIH-EDF) (see [1]). The execution time under the operating systems LinuX or Windows XP with 1 Mo free memory and 2 GHz CPU clock does not exceed a few seconds depending on the spatial mesh size and the final time desired.

5. Conclusion and perspectives

We have described in this paper a new method to simulate mixed flows and the related phenomena using a finite volumes method. The model and the numerical method reproduce correctly a laboratory test and can deal with multiple points of transition between the two type of flows. A current adaptation of this model is performed to deal with flows in convergent or divergent pipes. Another feature which is added is the dilatation of the pipe when the flow is pressurised. We have described the whole model in a recent article (see [1]) and it can be used to deal with this phenomenon. The last domain of investigation is the air entrapment phenomenon.

References

[1] C. Bourdarias, S. Gerbi, A conservative model for unsteady flows in deformable closed pipes and its implicit second order finite volume discretisation, Comput. & Fluids, submitted for publication.
[2] H. Capart, X. Sillen, Y. Zech, Numerical and experimental water transients in sewer pipes, J. Hydraul. Res. (1997) 659–672.
[3] J.A. Cunge, Comparison of physical and mathematical model test results on translation waves in the Oraison-Manosque power canal, La Houille Blanche (1966) 55–59.
[4] J.A. Cunge, M. Wegner, Intégration numérique des équations d'écoulement de Barré de Saint Venant par un schéma implicite de différences finies, La Houille Blanche (1964) 33–39.
[5] N.T. Dong, Sur une méthode numérique de calcul des écoulements non permanents soit à surface libre, soit en charge, soit partiellement à surface libre et partiellement en charge, La Houille Blanche (1990) 149–158.
[6] F. Dubois, An introduction to finite volumes, in: O. Pironneau, V. Shaidurov (Eds.), Computational Methods and Algorithms (Related chapters), Encyclopedia of Mathematical Sciences, vol. 2.6, Encyclopedia of Life Support Systems, 2001.
[7] R. Eymard, T. Gallouet, R. Herbin, The finite volume method, in: P. Ciarlet, J.L. Lions (Eds.), Handbook of Numerical Analysis, North-Holland, Amsterdam, 2000, pp. 713–1020, This paper appeared as a technical report four years ago.
[8] M. Fuamba, Contribution on transient flow modelling in storm sewers, J. Hydraul. Res. (2002) 685–693.
[9] T. Gallouet, J.M. Hérard, N. Seguin, Some approximate Godunov schemes to compute shallow-water equations with topography, Comput. Fluids 32 (2003) 479–513.
[10] T. Gallouet, J.M. Masella, Un schéma de Godunov approaché (a rough Godunov scheme), C. R. Acad. Sci. Ser. I 323 (1) (1996) 77–84.

[11] P. Garcia-Navarro, F. Alcrudo, A. Priestley, An implicit method for water flow modelling in channels and pipes, J. Hydraul. Res. (1994) 721–742.
[12] J.M. Greenberg, A.Y. LeRoux, A well balanced scheme for the numerical processing of source terms in hyperbolic equation, SIAM J. Numer. Anal. (1996) 1–16.
[13] M.A. Hamam, A. McCorquodale, Transient conditions in the transition from gravity to surcharged sewer flow, Can. J. Civ. Engrg. (1982) 189–196.
[14] A. Kumbaro, Modélisation, analyse mathématique et numérique des modèles bi-fluides d'écoulements diphasiques, Ph.D. Thesis, Université Paris XI, 1993.
[15] J. Li, A. McCorquodale, Modeling mixed flow in storm sewers, J. Hydraul. Engrg. (1999) 1170–1179.
[16] J.J. Morge, B.S. Garbow, K.E. Hillstrom, User Guide for MINPACK-1, Technical Report ANL-80-74, Argonne National Laboratory, March 1980.
[17] P.L. Roe, Some contributions to the modelling of discontinuous flow, in: B.E. Engquist, S. Osher, R.C.J. Somerville (Eds.), Large-scale Computations in Fluid Mechanics, Part 2. Proceedings of the 15th AMS-SIAM Summer Seminar on Applied Mathematics held at Scripps Institution of Oceanography, La Jolla, CA, June 27–July 8, 1983, Lectures in Applied Mathematics, vol. 22, American Mathematical Society, Providence, RI, 1985, pp. 163–193.
[18] A.Y. LeRoux, M.N. LeRoux, Convergence d'un schéma à profils stationnaires pour les équations quasi linéaires du premier ordre avec termes sources, C. R. Acad. Sci. Sér. I Math. 333 (7) (2001) 703–706.
[19] C.S.S. Song, Two-phase flow hydraulic transient model for storm sewer systems, in: Second International Conference on Pressure Surges, Bedford, England, 1976, pp. 17–34, BHRA Fluid engineering.
[20] C.S.S. Song, J.A. Cardle, K.S. Leung, Transient mixed-flow models for storm sewers, J. Hydraul. Engrg. ASCE (1983) 1487–1503.
[21] V.L. Streeter, E.B. Wylie, K.W. Bedford, Fluid Mechanics, McGraw-Hill, New York, 1998.
[22] D.B. Whitham, Linear and Nonlinear Waves, Wiley, New York, 1973.
[23] D.C. Wiggert, Transient flow in free surface, pressurized systems, J. Hydraul. Div. 98 (1) (1972) 11–27.